Journal of Computational and Applied Mathematics 236 (2011) 819–833

Contents lists available at SciVerse ScienceDirect

Journal of Computational and Applied Mathematics

journal homepage: www.elsevier.com/locate/cam

A numerical study of air–vapor–heat transport through textile materials with a moving interface☆

Q. Zhang [a,b], W. Sun [b,*]

[a] School of Mathematics and Computational Science, Sun Yat-Sen University, Guangzhou, China

[b] Department of Mathematics, City University of Hong Kong, Kowloon, Hong Kong, China

ARTICLE INFO

Keywords:
Multi-component flow
Clothing assemblies
Finite volume method
Moving interface

ABSTRACT

This paper focuses on the numerical study of heat and moisture transfer in clothing assemblies, which is described by a multi-component and multiphase air–vapor–heat flow with a moving interface. A splitting semi-implicit finite volume method is applied for the system of nonlinear parabolic equations and an implicit Euler scheme is used for the interface equation. In terms of classical Dirichlet to Neumann map, the implicit system can be solved directly and no iteration is needed. Two types of clothing assemblies are investigated and the comparison with experimental measurements is also presented.

1. Introduction

Heat and mass transfer in fibrous porous media attracts considerable attention since it can be found in a wide range of industrial and engineering domains [1–5]. A typical application in textile industry is a clothing assembly, consisting of a thick porous fibrous batting sandwiched by two thin fabrics. The outside cover of the assembly is exposed to a cold environment with fixed temperature and relative humidity while the inside cover is exposed to a mixture of air and vapor at higher temperature and relative humidity. Since the environment temperature is usually lower than freezing point, there is an interface arising in the batting area of clothing assembly. Therefore, this model, in other words, can be viewed as a two-phase Stefan type problem.

Numerical methods and simulations for heat and moisture transport in porous textile materials have been studied by many authors [6,2,7–11] with various applications. In [7], a classical finite difference method was applied for solving a single component model with thermal radiation, where the thermal radiation equation was solved analytically. A splitting finite volume method was proposed in [10] for the multiphase air–vapor–heat system. Several practical cases of clothing assemblies were studied in comparison with experimental data. The scheme used in [10] is semi-implicit in general. At each splitting step, a single component equation was solved with a semi-implicit scheme for this component and an explicit treatment for the other components. However, the interface was ignored in all these works, which resulted in the inaccuracy of numerical approximations and serious time step restriction. Numerical results presented in [10] show that the scheme requires the time step size to be smaller than 10 s.

In the past several decades, numerous efforts have been devoted to the study of numerical methods for moving interface problems, such as front tracking method, adaptive mesh method, level set method and immersed interface method [12–16]. The front tracking method is an explicit method in general, in which the interface is determined by a numerical solution

☆ The work of the authors was supported in part by a grant from the Research Grants Council of the Hong Kong Special Administrative Region, China (Project No. CityU 102409).

* Corresponding author.
E-mail addresses: mngq1118@yahoo.com.cn (Q. Zhang), maweiw@math.cityu.edu.hk (W. Sun).

0377-0427/$ – see front matter © 2011 Elsevier B.V. All rights reserved.
doi:10.1016/j.cam.2011.05.022

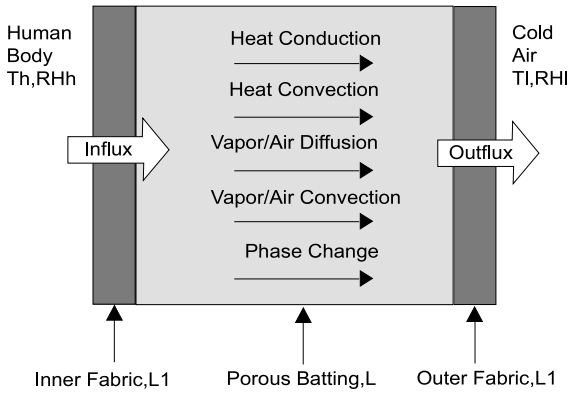

Fig. 1. Schematic diagram of the porous clothing assembly.

at an old time level and the heat (or other) equation is solved on a fixed mesh at a new time level. The adaptive moving mesh method has been studied by many authors [17,18]. In this method, the mesh points are controlled continuously and automatically by a mesh PDE which is employed to move the mesh to interfaces or singularities. The immersed finite difference method (IIM) was first proposed by LeVeque and Li [13] for solving steady state problems on regular meshes. The IIM method uses a standard finite difference approximation on mesh points away from interfaces while a special approximation with the interface condition embedding on mesh points near interfaces. Later, the method was extended to the Stefan problems with moving interfaces [19] and some other physical problems [14]. More recently, several immersed finite element and finite volume methods were introduced in [20,12] for solving steady state interface problems. Similarly, in the immersed FE methods, the standard FE basis functions are used in each of non-interface elements and in an interface element, local basis functions are constructed according to the interface such that these functions can satisfy jump conditions.

The main difficult from the classical Stefan problem is how to accurately determine the interface $\alpha(t)$, particularly for problems with a sharp interface and problems in which the solution is very sensitive to the interface. All existing approaches are based on either an explicit scheme and an implicit scheme with extra inner iterations for the interface equation since the flux jump is unknown in the new time level. In this paper, we present numerical study for a system of nonlinear, degenerate and strongly coupled parabolic equations with a moving interface, arising from air–vapor–heat transport in textile materials. A splitting finite volume method is proposed for the system. A Dirichlet to Neumann map type interface method (DNMIM) is applied for the interface equation of our model. We introduce an interface function, in terms of classical Dirichlet to Neumann map. The interface achieves at the zero of the interface function. Similar concepts may be found in [21–23] for some simple linear models. More important here is that the interface function at the new time level can be evaluated by a direct algorithm, and the interface location at the new time level can be determined without any inner iteration and extra cost. The computational complexity is almost same as that for solving the problem with a fixed boundary. Since the method is based on an implicit schedule for the interface equation, it is more stable than those based on an explicit one.

The rest of the paper is organized as follows. In Section 2, we introduce the mathematical model of heat–vapor–air transport in textile materials with a class of physical boundary conditions and an interface equation due to the temperature gradient jump and the jump of heat capacity. The model is described by a system of nonlinear, degenerate and strongly coupled parabolic equations. A new interface method then is introduced in Section 3 for the temperature equation and related interface equation involved in the system. In this method, the interface location at a new time level is determined by discrete Dirichlet to Neumann map. In Section 4, we present a splitting finite volume method with a semi-implicit Euler scheme in time direction and a second-order approximation in spatial direction. Some special compact approximations are introduced on the mesh points near the interface. In Section 5. we present an artificial example to test our algorithms, compared with some existing algorithms, and to confirm the accuracy of the proposed method. Numerical results show that the proposed method is much more stable than those methods with an explicit scheme for the interface equation. Finally, we apply the proposed method for solving the heat–vapor–air system. Clothing assemblies with 10 piles polyester batting and two different cover materials (nylon and laminated) are investigated numerically. The results are compared with experimental observations [24]. Numerical experiments show that the proposed method is efficient and stable almost unconditionally.

2. Mathematical model

Here we focus on heat and moisture transfer in a three-layer porous clothing assemblies as illustrated in Fig. 1, a thick porous fibrous batting sandwiched by two thin covers. The mathematical modeling of the heat and moisture transport has been studied by many authors and described usually by a multiphase and multi-component air–vapor–heat flow in the

porous textile materials. The model studied here is mainly based on the work in [10], which can be viewed as a generalization of models developed earlier in [1,2,7].

2.1. Mathematical equations

From the conservation of mass and energy, the physical process can be described by

$$\frac{\partial}{\partial t}(\epsilon C_v) + \frac{\partial}{\partial x}(u_g \epsilon C_v) - \frac{\partial}{\partial x}\left[\frac{D_g \epsilon}{\tau_c} C \frac{\partial}{\partial x}\left(\frac{C_v}{C}\right)\right] = -\Gamma, \tag{2.1}$$

$$\frac{\partial}{\partial t}(\epsilon C_a) + \frac{\partial}{\partial x}(u_g \epsilon C_a) - \frac{\partial}{\partial x}\left[\frac{D_g \epsilon}{\tau_c} C \frac{\partial}{\partial x}\left(\frac{C_a}{C}\right)\right] = 0, \tag{2.2}$$

$$\frac{\partial}{\partial t}(C_{vt} T) + \frac{\partial}{\partial x}\left(u_g \epsilon C C_{vg} T\right) - \frac{\partial}{\partial x}\left(\kappa \frac{\partial T}{\partial x}\right) = \lambda M \Gamma, \tag{2.3}$$

$$\frac{\partial}{\partial t}\left[\rho_f (1 - \epsilon')W\right] = M\Gamma. \tag{2.4}$$

Here the generalized Fick's law has been used for the binary multi-component gas mixture (vapor and air). C_v, C_a and $C = C_v + C_a$ are the water vapor, air and total (molar) concentrations, W is the liquid water content (%) relative to the fiber density, u_g is the molar averaged mixture velocity, τ_c is the tortuosity for the air–vapor diffusion, ρ_f is the density of fiber, M is the molecular weight of water and D_g is the molecular diffusion coefficient for air/vapor. In wet zone, λ is the latent heat of evaporation/condensation while in frozen zone, λ is the latent heat of sublimation.

The porosities with liquid water content (ϵ) and without liquid water content (ϵ') are related by

$$\epsilon = \epsilon' - \frac{\rho_f}{\rho_w} W(1 - \epsilon') \tag{2.5}$$

where ρ_w denotes the density of water.

The phase change rate due to the condensation/evaporation (molar rate) is defined by the Hertz–Knudsen equation [25]

$$\Gamma = -\frac{E}{R_f}\sqrt{\frac{(1-\epsilon)(1-\epsilon')}{2\pi RM}}\left(\frac{P_{\text{sat}} - P_v}{\sqrt{T}}\right) \tag{2.6}$$

where R is the universal gas constant and R_f is the radius of fiber, the saturation pressure P_{sat} is determined from experimental measurements [24] and the partial vapor pressure is given by

$$P_v = RC_v T. \tag{2.7}$$

The effective heat conductivity for gas–fiber–water mixture depends upon the conductivities of gas, vapor and water/ice, κ_g, κ_f and κ_w. A general form is given by

$$\kappa = \epsilon \kappa_g + (1 - \epsilon)\kappa_s \tag{2.8}$$

where

$$\kappa_s = \left(\kappa_f + \frac{\rho_f}{\rho_w} W \kappa_w\right)\left(1 + \frac{\rho_f}{\rho_w} W\right)^{-1}. \tag{2.9}$$

In the same way, the effective volumetric heat capacity can be obtained by

$$C_{vt} = \epsilon C_{vg} C + (1 - \epsilon) C_{vs} \tag{2.10}$$

where

$$C_{vs} = \left(C_{vf} + \frac{\rho_f}{\rho_w} W C_{vw}\right)\left(1 + \frac{\rho_f}{\rho_w} W\right)^{-1} \tag{2.11}$$

and C_{vg}, C_{vf} and C_{vw} are the heat capacities of the mixture gas, fiber and water/ice, respectively.

The vapor–air mixture velocity (volumetric discharge) is given by the Darcy's law

$$u_g = -\frac{k k_{rg}}{\mu_g}\frac{\partial P_g}{\partial x} \tag{2.12}$$

where k is the permeability, k_{rg} and μ_g are the relative permeability and the viscosity of the gas mixture, respectively. $P_g = P_v + P_a$ is the total gas pressure. k_{rg} can be obtained by the empirical relation $k_{rg} = (1 - s)^3$. Here, s is the volumetric liquid saturation in the inter-fiber void space, which is related to the water content by $s = (1 - \epsilon')\rho_f W/(\epsilon' \rho_w)$.

2.2. Boundary/initial conditions

Since the thickness of cover layers is much smaller than that of the batting layer, the properties of heat and moisture transfer in the covers are often described by simple resistances to heat, vapor and air transfer. A class of commonly used Robin type boundary conditions were introduced in [7] to approximate the experimental setup in [24], in which boundary conditions are defined by a combined simulation of cover layers and ambient environment. We use these Robin type boundary conditions in this paper.

At the outer boundary,

$$\begin{aligned} u_g\epsilon C_v - \frac{D_g\epsilon}{\tau_c}C\frac{\partial}{\partial x}\left(\frac{C_v}{C}\right)\Big|_{x=L} &= \frac{1}{R_v^o + 1/H_v^o}(C_v^o - C_v),\\ u_g\epsilon C_a - \frac{D_g\epsilon}{\tau_c}C\frac{\partial}{\partial x}\left(\frac{C_a}{C}\right)\Big|_{x=L} &= \frac{1}{R_a^o + 1/H_a^o}(C_a^o - C_a),\\ u_g\epsilon CC_{vg}T - \kappa\frac{\partial T}{\partial x}\Big|_{x=L} &= \frac{1}{R_t^o + 1/H_t^o}(T^o - T) \end{aligned} \tag{2.13}$$

where R_v^o, R_a^o and R_t^o are the resistances of the inner cover to vapor, air and heat. H_v^o and H_a^o are the mass transfer coefficients in the inner environment for vapor and air, respectively, and H_t^o is the heat transfer coefficient in the inner environment for heat.

We assume that the background temperature is fixed at T^o (e.g., -20 °C) with a relative humidity of RH^o (e.g., 70%). The background vapor and air concentrations can be calculated by

$$C_v^o = RH^o\frac{P_{\text{sat}}(T^o)}{RT^o}, \qquad C_a^o = \frac{P_{\text{atm}}}{RT^o}, \tag{2.14}$$

respectively, where P_{atm} is the atmospheric pressure.

Similar to the outer boundary, we have the following boundary conditions on the inner boundary

$$\begin{aligned} u_g\epsilon C_v - \frac{D_g\epsilon}{\tau_c}C\frac{\partial}{\partial x}\left(\frac{C_v}{C}\right)\Big|_{x=0} &= \frac{1}{R_v^i + 1/H_v^i}(C_v - C_v^i),\\ u_g\epsilon C_a - \frac{D_g\epsilon}{\tau_c}C\frac{\partial}{\partial x}\left(\frac{C_a}{C}\right)\Big|_{x=0} &= \frac{1}{R_a^i + 1/H_a^i}(C_a - C_a^i),\\ u_g\epsilon CC_{vg}T - \kappa\frac{\partial T}{\partial x}\Big|_{x=0} &= \frac{1}{R_t^i + 1/H_t^i}(T - T^i) \end{aligned} \tag{2.15}$$

where R_v^i, R_a^i, R_t^i, H_v^i, H_a^i, H_v^i and H_t^i are defined analogously. Also we assume a relative humidity at the inner environment is 100% due to a constant evaporation, i.e., $RH^i = 1$. The vapor concentration can be computed by

$$C_v^i = RH^i\frac{P_{\text{sat}}(T^i)}{RT^i} \tag{2.16}$$

where T^i is the inner background temperature.

The initial conditions are given by

$$T = 25\ ^\circ\text{C}, \qquad C_v = 65\%\frac{P_{\text{sat}}(T)}{RT}, \qquad C_a = \frac{P_{\text{atm}}}{RT}, \qquad W = 0, \quad \text{for } t = 0. \tag{2.17}$$

2.3. Interface equation

When the outer cover of the assembly is exposed to a cold environment under the freezing point and the inner cover is exposed at a higher temperature (e.g., human skin), there are a wet zone and a frozen zone in the batting area. A moving interface occurs at the position of the freezing temperature $T_f = 273$ K. Since the amount of the water content (sweat) in assemblies is relative small, the difference between the densities of water and ice will be neglected. Therefore, the porosity ϵ and the relative permeability k_{rg} are continuous at the interface. The interface arises mainly due to the jump of the heat capacity C_{vt} (more precisely C_{vs}), the heat conductivity κ and latent heat λ at the freezing point. In this case, the temperature equation should be discretized with some special treatment around the moving interface. By classical formulas of two-phase flow [26], the interface location $\alpha(t)$ satisfies the following interface equation

$$((1-\epsilon)\lambda_{wi}\rho_f W - [C_{vt}]T_f)\alpha_t = [\kappa T_x] \tag{2.18}$$

where $[u]$ denotes the jump of u at the interface, ρ_f denotes the density of fiber, W is the liquid water content, λ_{wi} is the phase change latent heat from water to ice. Finally we assume that the interface curve is smooth and satisfies the following condition

$$|\alpha'(t)| \geq \underline{\alpha} > 0 \tag{2.19}$$

for some positive constant $\underline{\alpha}$.

With non-dimensionalization, we rewrite the system (2.1)–(2.4) by

$$\frac{\partial}{\partial t}\left[\rho_f(1-\epsilon')W\right] = M\Gamma_C \tag{2.20}$$

$$\frac{\partial}{\partial t}\left(\frac{\epsilon P}{RT}\right) + \frac{\partial}{\partial x}\left(V_G C\frac{\partial P}{\partial x}\right) = -\Gamma_C \tag{2.21}$$

$$\frac{\partial}{\partial t}(\epsilon C_v) + \frac{\partial}{\partial x}\left(V_G\frac{\partial P}{\partial x}C_v\right) - \frac{\partial}{\partial x}\left[D_G C\frac{\partial}{\partial x}\left(\frac{C_v}{C}\right)\right] = -\Gamma_C \tag{2.22}$$

$$\epsilon C C_{vg}\frac{\partial T}{\partial t} + \frac{\partial(C_{vs}(1-\epsilon)T)}{\partial t} - V_T C\frac{\partial P}{\partial x}\frac{\partial T}{\partial x} - \frac{\partial}{\partial x}\left(\kappa\frac{\partial T}{\partial x}\right) = \Gamma_T \tag{2.23}$$

where

$$V_G = \frac{k\epsilon(1-s)^3}{\mu_g}, \qquad D_G = \frac{\epsilon D_a}{\tau_c}, \qquad \beta = \frac{E(1-\epsilon')}{R_f\sqrt{2\pi RM}}\sqrt{1+\frac{\rho_f}{\rho_w}W}$$

$$V_T = C_{vg}V_G, \qquad \Gamma_c = \beta\frac{RC_vT - P_{\text{sat}}}{\sqrt{T}}, \qquad \Gamma_T = (\lambda M + C_{vg}T)\Gamma_c.$$

Eq. (2.21) is obtained by adding Eqs. (2.1) and (2.2) together where we have introduced the pressure $P = RCT$ as a main variable as usual. Eq. (2.23) is obtained by combining the Eqs. (2.3) and (2.21).

The corresponding boundary conditions are defined by

$$\begin{aligned}
&-V_G\frac{\partial P}{\partial x}\frac{P}{RT}\bigg|_{x=0} = \beta_{11}^0(C_v - C_v^i) + \beta_{12}^0(C_a - C_a^i),\\
&-V_G\frac{\partial P}{\partial x}C_v - D_G C\frac{\partial}{\partial x}\left(\frac{C_v}{C}\right)\bigg|_{x=0} = \beta_{21}^0(C_v - C_v^i),\\
&-V_T C\frac{\partial P}{\partial x}T - \kappa\frac{\partial T}{\partial x}\bigg|_{x=0} = \beta_{31}^0(T - T^i)
\end{aligned} \tag{2.24}$$

at $x = 0$ and

$$\begin{aligned}
&-V_G\frac{\partial P}{\partial x}\frac{P}{RT}\bigg|_{x=L} = \beta_{11}^L(C_v^o - C_v) + \beta_{12}^L(C_a^o - C_a),\\
&-V_G\frac{\partial P}{\partial x}C_v - D_G C\frac{\partial}{\partial x}\left(\frac{C_v}{C}\right)\bigg|_{x=L} = \beta_{21}^L(C_v^o - C_v),\\
&-V_T C\frac{\partial P}{\partial x}T - \kappa\frac{\partial T}{\partial x}\bigg|_{x=L} = \beta_{31}^L(T^o - T)
\end{aligned} \tag{2.25}$$

at $x = L$.

3. A numerical method for the temperature equation with a moving interface

Numerical study for problems with a moving interface has been studied by many authors [12,13,19,14]. Due to the high nonlinearity of the model and the practical interest in a long time period, a stable scheme with less cost and large time step is preferable. In this section, we shall combine the semi-implicit splitting finite volume method proposed in [10] with a fast interface algorithm for the heat–air–vapor system. The fast interface algorithm can capture the interface more accurate without any iteration and also make the scheme more stable.

3.1. Numerical discretization

Let $\{x_j\}_{j=0}^{M+1}$ be a uniform mesh on $[0, L]$ with the mesh size h and $\{t_n\}_{n=0}^{N}$ be a uniform mesh in the time direction with the step size τ. For any mesh function $\{u_j\}$, we denote

$$u_{j+1/2} = (u_j + u_{j+1})/2, \qquad \delta_x u_{j+1/2} = (u_{j+1} - u_j)/h.$$

We assume that the interface $\alpha_n \in (x_{k_n}, x_{k_n+1})$. Since the interface may cross several grid lines during one time step, with a modified semi-implicit Euler scheme in time direction, the discrete temperature equations at regular points are defined by

$$\begin{aligned} &C_{vg}C_j^n\epsilon_j^n\frac{T_j^{n+1}-\hat{T}_j^n}{\hat{\tau}} + \frac{C_{s,j}^{n+1}(1-\epsilon_j^{n+1})T_j^{n+1} - C_{s,j}^n(1-\epsilon_j^n)\hat{T}_j^n}{\hat{\tau}} = L_h^T(T_j^{n+1}, x_j) + \Gamma_{T,j}^n \\ &\quad + \frac{\partial \Gamma_T}{\partial T}\bigg|_{T=T_j^n}(T_j^{n+1} - T_j^n), \quad j = 1, 2, \ldots, k_{n+1}-1, k_{n+1}+2, \ldots, M;\ n = 0, 1, \ldots, N \end{aligned} \tag{3.1}$$

where $V_j^n = (P_{j+1}^n - P_{j-1}^n)/(2h)$ and

$$L_h^T(T_j^{n+1}, x_j) := V_{T,j}^n C_j^n V_j^n \frac{T_{j+1}^{n+1} - T_{j-1}^{n+1}}{2h} + \frac{1}{h}\left(\kappa_{j+1/2}^n \delta_x T_{j+1/2}^{n+1} - \kappa_{j-1/2}^n \delta_x T_{j-1/2}^{n+1}\right), \tag{3.2}$$

$$\begin{aligned} &\hat{T}_j^n = T_j^n, \qquad \hat{\tau} = \tau, \quad \text{for } j > k_n \quad \text{and} \quad j < k_{n+1}+1, \quad \text{if } \alpha_{n+1} \le \alpha_n, \\ &\hat{T}_j^n = T_f, \qquad \hat{\tau} = \tau\frac{\alpha_{n+1} - x_j}{\alpha_{n+1} - \alpha_n} \quad \text{for } k_{n+1}+1 \le j \le k_n, \quad \text{if } \alpha_{n+1} \le \alpha_n, \\ &\hat{T}_j^n = T_j^n, \qquad \hat{\tau} = \tau, \quad \text{for } j \le k_n \quad \text{and} \quad j \ge k_{n+1}+1, \quad \text{if } \alpha_{n+1} > \alpha_n, \\ &\hat{T}_j^n = T_f, \qquad \hat{\tau} = \tau\frac{\alpha_{n+1} - x_j}{\alpha_{n+1} - \alpha_n} \quad \text{for } k_n+1 \le j \le k_{n+1}, \quad \text{if } \alpha_{n+1} > \alpha_n. \end{aligned}$$

Since the source term (2.6) is nonlinear for temperature, a simple linearization of the source term has been used in (3.1).

The corresponding finite volume type boundary conditions are given by

$$\begin{aligned} &\epsilon_0^n C_{vg}C_0^n(T_0^{n+1} - T_0^n) + (1-\epsilon_0^{n+1})C_{s,0}^{n+1}T_0^{n+1} - (1-\epsilon_0^n)C_{s,0}^n T_0^n \\ &\quad = \frac{2\tau}{h}\left[V_{T,1/2}^n C_{1/2}^n \delta_x P_{1/2}^n \delta_x T_{1/2}^{n+1} + \kappa_{1/2}^n \delta_x T_{1/2}^{n+1} - \beta_{31}^0(T_0^{n+1} - T^i)\right] + \tau\frac{\partial \Gamma_T}{\partial T}\bigg|_{T=T_0^n}(T_0^{n+1} - T_0^n) + \tau\Gamma_{T,0}^n, \end{aligned} \tag{3.3}$$

at $x = 0$ and

$$\begin{aligned} &\epsilon_M^n C_{vg}C_M^n(T_M^{n+1} - T_M^n) + (1-\epsilon_M^{n+1})C_{s,M}^{n+1}T_M^{n+1} - (1-\epsilon_M^n)C_{s,M}^n T_M^n \\ &\quad = -\frac{2\tau}{h}\left[V_{T,M-1/2}^n C_{M-1/2}^n \delta_x P_{M-1/2}^n \delta_x T_{M-1/2}^{n+1} + \kappa_{M-1/2}^n \delta_x T_{M-1/2}^{n+1} + \beta_{31}^L(T^o - T_M^{n+1})\right] \\ &\qquad + \tau\frac{\partial \Gamma_T}{\partial T}\bigg|_{T=T_M^n}(T_M^{n+1} - T_M^n) + \tau\Gamma_{T,M} \end{aligned} \tag{3.4}$$

at $x = L$.

3.2. A direct algorithm for the interface location

From the interface equation (2.18), we have

$$\alpha(t) = \alpha(t_n) + \int_{t_n}^{t} \widetilde{\lambda}[\kappa T_x]dt \tag{3.5}$$

where $\widetilde{\lambda} = ((1-\epsilon)\lambda_{wi}\rho_f W_f - [C_{vt}]T_f)^{-1}$. We define an interface function by

$$J^n(y) = y(t) - \left(\alpha(t_n) + \int_{t_n}^{t_{n+1}} \widetilde{\lambda}[\kappa T_x]dt\right) \tag{3.6}$$

where $y = y(t)$ denotes a curve connecting the points $(\alpha(t_n), t_n)$ and (y, t_{n+1}). Clearly, we have

$$J^n(\alpha(t_{n+1})) = 0.$$

To approximate the interface function, we use the trapezoidal rule (Crank–Nicolson scheme) and the discrete scheme is given by

$$J_k^n := x_k - \alpha_n - \frac{\tau}{2}\left(\widetilde{\lambda}[\kappa T_x](\alpha_n, t_n) + \widetilde{\lambda}[\kappa T_x](x_k, t_{n+1})\right). \tag{3.7}$$

Under the assumption (2.19), J_k^n can be used to determine the location of the interface. If $J_k^n = 0$ for some k, the numerical interface point at the new time step is $\alpha_{n+1} = x_k$. In general, we need to find a subinterval (x_k, x_{k+1}) with $J_k^n J_{k+1}^n < 0$.

To calculate J_k^n by (3.7), one needs to evaluate the flux jump $\{\widetilde{\lambda}[\kappa T_x](x_k, t_{n+1})\}$ by solving discrete temperature systems defined in $[0, x_k]$ and $[x_k, L]$, respectively, with the Dirichlet boundary condition

$$T(x_k, t_{n+1}) = T_f := 273\ \text{K}.$$

Let $\{\bar{T}_j^{n+1}\}_{j=1}^{k-1}$ and $\{\bar{T}_j^{n+1}\}_{j=k+1}^{M-1}$ be the solution of the temperature equation in $[0, x_k]$ and $[x_k, L]$, respectively. We can rewrite the corresponding finite volume system by

$$A^{\pm} v^{\pm} = d^{\pm}$$

or equivalently,

$$\begin{aligned} &a_j^- \bar{T}_{j-1}^{n+1} + b_j^- \bar{T}_j^{n+1} + c_j^- \bar{T}_{j+1}^{n+1} = d_j^-, \quad j = 1, \ldots, k-1, \\ &a_j^+ \bar{T}_{j-1}^{n+1} + b_j^+ \bar{T}_j^{n+1} + c_j^+ \bar{T}_{j+1}^{n+1} = d_j^+ \quad j = k+1, k+2, \ldots, M \end{aligned} \tag{3.8}$$

where $a_1^- = c_{k-1}^- = a_{k+1}^+ = c_M^+ = 0$. Using the backward and forward Gaussian eliminations for the left and right systems, respectively, reduces these two tridiagonal systems to two systems of upper and lower bi-diagonal structures

$$\begin{bmatrix} \bar{b}_1^- & \bar{c}_1^- & & & \\ & \bar{b}_2^- & \bar{c}_2^- & & \\ & & \ddots & \ddots & \\ & & & \bar{b}_{k-2}^- & \bar{c}_{k-2}^- \\ & & & & \bar{b}_{k-1}^- \end{bmatrix}_{(k-1)\times(k-1)}, \quad \text{and} \quad \begin{bmatrix} \bar{b}_{k+1}^+ & & & & \\ \bar{a}_{k+2}^+ & \bar{b}_{k+2}^+ & & & \\ & \ddots & \ddots & & \\ & & & \bar{b}_{M-1}^+ & 0 \\ & & & \bar{a}_M^+ & \bar{b}_M^+ \end{bmatrix}_{(M-k)\times(M-k)} \tag{3.9}$$

from which we can calculate $\bar{T}_{k-1}^{n+1}$, $\bar{T}_{k-2}^{n+1}$ and $\bar{T}_{k+1}^{n+1}$, $\bar{T}_{k+2}^{n+1}$ (not all components). An approximation to the flux at x_k^- is given by

$$(\kappa \bar{T}_x)(x_k^-, t_{n+1}) \approx \kappa(x_k^-, t_{n+1}) \frac{\bar{T}_{k-2}^{n+1} - 4\bar{T}_{k-1}^{n+1} + 3\bar{T}_f}{2h} \tag{3.10}$$

and similarly,

$$(\kappa \bar{T}_x)(x_k^+, t_{n+1}) \approx -\kappa(x_k^+, t_{n+1}) \frac{\bar{T}_{k+2}^{n+1} - 4\bar{T}_{k+1}^{n+1} + 3\bar{T}_f}{2h} \tag{3.11}$$

from which we can calculate the flux jump $[\kappa \bar{T}_x](x_k, t_{n+1})$. Moreover, we evaluate the interface function J_k^n by (3.7).

Finally, we can find an interval $[x_{k_{n+1}}, x_{k_{n+1}+1}]$ with

$$J_{k_{n+1}}^n J_{k_{n+1}+1}^n < 0. \tag{3.12}$$

By a simple linear interpolation, the flux jump at the interface $x = \alpha_{n+1}$ can be calculated from the following formula,

$$[\kappa T_x](\alpha_{n+1}, t_{n+1}) \approx \frac{\alpha_{n+1} - x_{k_{n+1}}}{h} [\kappa \bar{T}_x](x_{k_{n+1}+1}, t_{n+1}) + \frac{x_{k_{n+1}+1} - \alpha_{n+1}}{h} [\kappa \bar{T}_x](x_{k_{n+1}}, t_{n+1}). \tag{3.13}$$

By (3.5), we get

$$\alpha_{n+1} - \alpha_n = \frac{\tau}{2}\left[\widetilde{\lambda}[\kappa T_x](\alpha_n, t_n) + \frac{\alpha_{n+1} - x_{k_{n+1}}}{h} \widetilde{\lambda}[\kappa \bar{T}_x](x_{k_{n+1}+1}, t_{n+1}) + \frac{x_{k_{n+1}+1} - \alpha_{n+1}}{h} \widetilde{\lambda}[\kappa \bar{T}_x](x_{k_{n+1}}, t_{n+1})\right],$$

from which, we find the interface α_{n+1} by

$$\alpha_{n+1} = \frac{\alpha_n + \frac{\tau}{2}\widetilde{\lambda}[\kappa T_x](\alpha_n, t_n) - \frac{\tau}{2h} x_{k_{n+1}} \widetilde{\lambda}[\kappa \bar{T}_x](x_{k_{n+1}+1}, t_{n+1}) + \frac{\tau}{2h} x_{k_{n+1}+1} \widetilde{\lambda}[\kappa \bar{T}_x](x_{k_{n+1}}, t_{n+1})}{1 - \frac{\tau}{2h}\widetilde{\lambda}[\kappa \bar{T}_x](x_{k_{n+1}+1}, t_{n+1}) + \frac{\tau}{2h}\widetilde{\lambda}[\kappa \bar{T}_x](x_{k_{n+1}}, t_{n+1})}. \tag{3.14}$$

3.3. An algorithm for temperature equation

After the interface location is determined by (3.14), we need to solve the temperature equation at $t = t_{n+1}$ in the intervals $[0, \alpha_{n+1}]$ and $[\alpha_{n+1}, L]$, respectively, with the Dirichlet boundary condition $T(\alpha_{n+1}, t_{n+1}) = T_f$.

Since α_{n+1} may not be a mesh point, we have to modify the finite difference system (3.1) at the mesh points near the interface. A second-order approximation to T_{xx} at $x_l = (x_{k_{n+1}-1} + x_{k_{n+1}} + \alpha_{n+1})/3$ and $x_r = (\alpha_{n+1} + x_{k_{n+1}+1} + x_{k_{n+1}+2})/3$ is defined by

$$\begin{aligned}
T_{xx}(x_l, t_{n+1}) &= \frac{2}{(\alpha_{n+1} - x_{k_{n+1}-1})h} T(x_{k_{n+1}-1}, t_{n+1}) - \frac{2}{(\alpha_{n+1} - x_{k_{n+1}})h} T(x_{k_{n+1}}, t_{n+1}) \\
&\quad + \frac{2}{(\alpha_{n+1} - x_{k_{n+1}})(\alpha_{n+1} - x_{k_{n+1}-1})} T_f + O(h^2), \\
T_{xx}(x_r, t_{n+1}) &= \frac{2}{(\alpha_{n+1} - x_{k_{n+1}+1})h} T(x_{k_{n+1}+1}, t_{n+1}) - \frac{2}{(\alpha_{n+1} - x_{k_{n+1}+2})h} T(x_{k_{n+1}+2}, t_{n+1}) \\
&\quad + \frac{2}{(\alpha_{n+1} - x_{k_{n+1}+1})(\alpha_{n+1} - x_{k_{n+1}+2})} T_f + O(h^2),
\end{aligned} \tag{3.15}$$

respectively. Also we construct an approximation to T_x in terms of the values at these three points by

$$\begin{aligned}
T_x(x_l, t_{n+1}) &= -\frac{(x_l - x_{k_{n+1}-1})(\alpha_{n+1} - x_{k_{n+1}}) + (x_{k_{n+1}} - x_l)(\alpha_{n+1} - x_{k_{n+1}-2})}{h^2(\alpha_{n+1} - x_{k_{n+1}-1})} T(x_{k_{n+1}-1}, t_{n+1}) \\
&\quad + \frac{(x_l - x_{k_{n+1}-1})(\alpha_{n+1} - x_{k_{n+1}+1}) + (x_{k_{n+1}} - x_l)(\alpha_{n+1} - x_{k_{n+1}-1})}{h^2(\alpha_{n+1} - x_{k_{n+1}})} T(x_{k_{n+1}}, t_{n+1}) \\
&\quad + \frac{2x_l - x_{k_{n+1}-1} - x_{k_{n+1}}}{(\alpha_{n+1} - x_{k_{n+1}-1})(\alpha_{n+1} - x_{k_{n+1}})} T_f + O(h^2). \\
T_x(x_r, t_{n+1}) &= -\frac{(x_r - x_{k_{n+1}+1})(\alpha_{n+1} - x_{k_{n+1}+2}) + (x_{k_{n+1}+2} - x_r)(\alpha_{n+1} - x_{k_{n+1}})}{h^2(\alpha_{n+1} - x_{k_{n+1}+1})} T(x_{k_{n+1}+1} =, t_{n+1}) \\
&\quad + \frac{(x_r - x_{k_{n+1}+1})(\alpha_{n+1} - x_{k_{n+1}+3}) + (x_{k_{n+1}+2} - x_r)(\alpha_{n+1} - x_{k_{n+1}+1})}{h^2(\alpha_{n+1} - x_{k_{n+1}+2})} T(x_{k_{n+1}+2}, t_{n+1}) \\
&\quad + \frac{2x_r - x_{k_{n+1}+1} - x_{k_{n+1}+2}}{(\alpha_{n+1} - x_{k_{n+1}+1})(\alpha_{n+1} - x_{k_{n+1}+2})} T_f + O(h^2).
\end{aligned} \tag{3.16}$$

With these approximations we can obtain the discrete approximations to $L_h(T_j^{n+1}, x_l)$ and $L_h(T_j^{n+1}, x_r)$. Finally two discrete equations at (x_l, t_{n+1}) and (x_r, t_{n+1}) are given by

$$\begin{aligned}
&\frac{x_{k_{n+1}} - x_l}{h} \left(C_{vg} C^n \epsilon^n \frac{T^{n+1} - \hat{T}^n}{\hat{\tau}} + \frac{C_s^{n+1}(1 - \epsilon^{n+1})T^{n+1} - C_s^n(1 - \epsilon^n)\hat{T}^n}{\hat{\tau}} \right) \Bigg|_{x_{k_{n+1}-1}} \\
&\quad + \frac{x_l - x_{k_{n+1}-1}}{h} \left(C_{vg} C^n \epsilon^n \frac{T^{n+1} - \hat{T}^n}{\hat{\tau}} + \frac{C_s^{n+1}(1 - \epsilon^{n+1})T^{n+1} - C_s^n(1 - \epsilon^n)\hat{T}^n}{\hat{\tau}} \right) \Bigg|_{x_{k_{n+1}}} \\
&= L_h^T(T_j^{n+1}, x_l) + \frac{x_{k_{n+1}} - x_l}{h} \left(\frac{\partial \Gamma_T}{\partial T} \Big|_{T=T^n} (T^{n+1} - T^n) + \Gamma_T^n \right) \Bigg|_{x_{k_{n+1}-1}} \\
&\quad + \frac{x_l - x_{k_{n+1}-1}}{h} \left(\frac{\partial \Gamma_T}{\partial T} \Big|_{T=T^n} (T^{n+1} - T^n) + \Gamma_T^n \right) \Bigg|_{x_{k_{n+1}}}
\end{aligned} \tag{3.17}$$

and

$$\begin{aligned}
&\frac{x_{k_{n+1}+2} - x_r}{h} \left(C_{vg} C^n \epsilon^n \frac{T^{n+1} - \hat{T}^n}{\hat{\tau}} + \frac{C_s^{n+1}(1 - \epsilon^{n+1})T^{n+1} - C_s^n(1 - \epsilon^n)\hat{T}^n}{\hat{\tau}} \right) \Bigg|_{x_{k_{n+1}+1}} \\
&\quad + \frac{x_r - x_{k_{n+1}+1}}{h} \left(C_{vg} C^n \epsilon^n \frac{T^{n+1} - \hat{T}^n}{\hat{\tau}} + \frac{C_s^{n+1}(1 - \epsilon^{n+1})T^{n+1} - C_s^n(1 - \epsilon^n)\hat{T}^n}{\hat{\tau}} \right) \Bigg|_{x_{k_{n+1}+2}}
\end{aligned}$$

$$= L_h^T(T_j^{n+1}, x_r) + \frac{x_{k_{n+1}+2} - x_r}{h}\left(\frac{\partial \Gamma_T}{\partial T}\bigg|_{T=T^n}(T^{n+1} - T^n) + \Gamma_T^n\right)\bigg|_{x_{k_{n+1}+1}}$$

$$+ \frac{x_l - x_{k_{n+1}+1}}{h}\left(\frac{\partial \Gamma_T}{\partial T}\bigg|_{T=T^n}(T^{n+1} - T^n) + \Gamma_T^n\right)\bigg|_{x_{k_{n+1}+2}} \tag{3.18}$$

which, in a simple form, are rewritten by

$$\bar{a}^-_{k_{n+1}} T^{n+1}_{k_{n+1}-1} + \bar{b}^-_{k_{n+1}} T^{n+1}_{k_{n+1}} = \bar{d}_{k_{n+1}-1}$$
$$\bar{b}^+_{k_{n+1}+1} T^{n+1}_{k_{n+1}+1} + \bar{c}^+_{k_{n+1}+1} T^{n+1}_{k_{n+1}+2} = \bar{d}_{k_{n+1}+1}.$$

More important here is that we do not need to re-solve these two systems. By noting these two bi-diagonal systems in (3.9), we obtain the following two almost bi-diagonal systems immediately

$$A^{\pm} T^{n+1}_{\pm} = d^{\pm} \tag{3.19}$$

where

$$A^- = \begin{bmatrix} \bar{b}^-_1 & \bar{c}^-_1 & & \\ & \ddots & \ddots & \\ & & \bar{b}^-_{k_{n+1}-1} & \bar{c}^-_{k_{n+1}-1} \\ & & \bar{a}^-_{k_{n+1}} & \bar{b}^-_{k_{n+1}} \end{bmatrix}_{k_{n+1}\times k_{n+1}} \quad A^+ = \begin{bmatrix} \bar{b}^+_{k_{n+1}+1} & \bar{c}^+_{k_{n+1}+1} & & \\ \bar{a}^+_{k_{n+1}+2} & \bar{b}^+_{k_{n+1}+2} & & \\ & \ddots & \ddots & \\ & & \bar{a}^+_M & \bar{b}^+_M \end{bmatrix}_{(M-k_{n+1})\times(M-k_{n+1})}.$$

Solving these two system gives the finite volume solution of the temperature equation at $t = t_{n+1}$.

We present the interface algorithm below.

Algorithm I.

- Step 1. Generate the tridiagonal system (3.8). Assume that $\alpha(t_{n+1}) \in [x_{k_n+p_1}, x_{k_n+p_2}]$ for certain integers p_1 and p_2. Generate the upper bi-diagonal matrix in (3.9) until $k = k_n+p_2$ and the lower bi-diagonal matrix in (3.9) until $k = k_n+p_1$, by the forward and backward Gaussian eliminations, respectively.
- Step 2. Evaluate the flux jump $\{\tilde{\lambda}[\kappa \bar{T}_x](x_k, t_{n+1})\}$ and the interface function $\{J_k^n\}$. Then find an interval containing the interface by using (3.12) and capture the location of interface at new time step by (3.14).
- Step 3. Calculate $\bar{a}^-_{k_{n+1}-1}$, $\bar{b}^-_{k_{n+1}-1}$, $\bar{b}^+_{k_{n+1}+1}$ and $\bar{c}^+_{k_{n+1}+1}$ in (3.17) and (3.18) and solve these two almost bi-diagonal systems in (3.19) for the finite volume solution T_j^{n+1}.

4. Numerical discretization for other equations

In this section, we introduce a splitting semi-implicit finite volume method for Eqs. (2.20)–(2.22). In each splitting step, one only needs to solve a single component equation with a semi-implicit scheme for this component and an explicit treatment for other components. After the interface is determined, the equations for other components can be viewed as boundary value problems with a fixed interface.

Let P_j^n, $C_{v,j}^n$, and W_j^n the numerical solutions of the pressure, vapor concentration, and water/ice content at the control volume (x_j, x_{j+1}) and $t = t_n$, respectively. A regular finite volume discretization can be obtained on the basis of integral form of the flux conservation in the spatial cell $(x_{j-1/2}, x_{j+1/2})$ and the time interval (t_n, t_{n+1}) when the cell is not close to the interface. The detailed derivation for general finite volume methods can be found in [10].

For the water equation (2.20), since the source is continuous, the discrete water system is given by

$$\frac{\rho_f(1-\epsilon')}{\tau}(W_j^{n+1} - W_j^n) = M\Gamma_{c,j}^n, \quad j = 1, 2, \ldots, M. \tag{4.1}$$

For the pressure equation (2.21), we have the interface condition

$$[P](\alpha(t), t) = [P_x](\alpha(t), t) = 0.$$

For simplicity, we assume that $\alpha_n < \alpha_{n+1}$ and $\alpha_{n+1} \in (x_{k_{n+1}}, x_{k_{n+1}+1})$. The discrete pressure equations at regular points are defined by

$$\frac{1}{\tau}\left(\epsilon_j^{n+1}\frac{P_j^{n+1}}{RT_j^{n+1}} - \epsilon_j^n \frac{P_j^n}{RT_j^n}\right) + L_h^P(P_j^{n+1}, x_j) = -\Gamma_{c,j}^n, \quad j = 1, 2, \ldots, k_n, k_{n+1}+2, \ldots, M \tag{4.2}$$

where

$$L_h^P(P_j^{n+1}, x_j) := \frac{1}{h}\left[V_{G,j+1/2}^n C_{j+1/2}^n \delta_x P_{j+1/2}^{n+1} - V_{G,j-1/2}^n C_{j-1/2}^n \delta_x P_{j-1/2}^{n+1}\right]. \tag{4.3}$$

When $k_n < k_{n+1}$, i.e., the interface crosses the spatial mesh line, we use the following implicit/explicit scheme on mesh points around the interface

$$\frac{1}{\tau_1}\left(\epsilon_j^{n+1}\frac{P_j^{n+1}}{RT_j^{n+1}}-\epsilon_j^{n}\frac{P_j^{n+\tau_2}}{RT_j^{n+\tau_2}}\right)+L_h^P(P_j^{n+1},x_j)=-\Gamma_{c,j}^n,\quad j=k_n+1,\ldots,k_{n+1}-1$$
$$\frac{1}{\tau_2}\left(\epsilon_j^{n+1}\frac{P_j^{n+\tau_2}}{RT_j^{n+\tau_2}}-\epsilon_j^{n}\frac{P_j^{n}}{RT_j^{n}}\right)+L_h^P(P_j^{n},x_j)=-\Gamma_{c,j}^n,\quad j=k_n+1,\ldots,k_{n+1}-1$$

which further produces

$$\frac{1}{\tau}\left(\epsilon_j^{n+1}\frac{P_j^{n+1}}{RT_j^{n+1}}-\epsilon_j^{n}\frac{P_j^{n}}{RT_j^{n}}\right)+\frac{\tau_1}{\tau}L_h^P(P_j^{n+1},x_j)+\frac{\tau_2}{\tau}L_h^P(P_j^{n},x_j)=-\Gamma_{c,j}^n,\quad j=k_n+1,\ldots,k_{n+1}-1 \tag{4.4}$$

where $\tau_1=t_{n+1}-t_j^\alpha$, $\tau_2=t_j^\alpha-t_n$ and $x_j=\alpha(t_j^\alpha)$. We apply the second-order approximation presented in (3.15) and (3.16) to get two more discrete equations at the points x_l and x_r, which is defined in a simple form by

$$(V_GP_x)_x(x_l,t_{n+1})=\gamma_{21}^-P_{k_{n+1}-1}^{n+1}+\gamma_{22}^-P_{k_{n+1}}^{n+1}+\gamma_{23}^-P_f^{n+1}:=L_h^P(P_j^{n+1},x_l)$$
$$(V_GP_x)_x(x_r,t_{n+1})=\gamma_{21}^+P_f^{n+1}+\gamma_{22}^+P_{k_{n+1}+1}^{n+1}+\gamma_{23}^+P_{k_{n+1}+2}^{n+1}:=L_h^P(P_j^{n+1},x_r). \tag{4.5}$$

Similarly, we can obtain a second-order approximation to $P_x(\alpha_{n+1}^{\pm},t_{n+1})$

$$P_x(\alpha_{n+1}^-,t_{n+1})=\gamma_{11}^-P_{k_{n+1}-1}^{n+1}+\gamma_{12}^-P_{k_{n+1}}^{n+1}+\gamma_{13}^-P_f^{n+1}$$
$$P_x(\alpha_{n+1}^+,t_{n+1})=\gamma_{11}^+P_f^{n+1}+\gamma_{12}^+P_{k_{n+1}+1}^{n+1}+\gamma_{13}^+P_{k_{n+1}+2}^{n+1}$$

where $P_f^{n+1}=P(\alpha(t_{n+1}),t_{n+1})$. With the interface condition $[P_x]=0$, we further have

$$P_f^{n+1}=\frac{\gamma_{11}^-P_{k_{n+1}-1}^{n+1}+\gamma_{12}^-P_{k_{n+1}}^{n+1}-\gamma_{12}^+P_{k_{n+1}+1}^{n+1}-\gamma_{13}^+P_{k_{n+1}+2}^{n+1}}{\gamma_{13}^--\gamma_{11}^+}.$$

Combining the last five equations leads to a second-order approximation to $L_h^P(P_j^{n+1},x_l)$ and $L_h^P(P_j^{n+1},x_r)$, respectively, and consequently, two discrete equations at (x_l,t_{n+1}) and (x_r,t_{n+1}) are given by

$$\frac{x_{k_{n+1}}-x_l}{h\tau}\left(\epsilon^{n+1}\frac{P^{n+1}}{RT^{n+1}}-\epsilon^{n}\frac{P^{n}}{RT^{n}}\right)\Big|_{x_{k_{n+1}-1}}+\frac{x_l-x_{k_{n+1}-1}}{h\tau}\left(\epsilon^{n+1}\frac{P^{n+1}}{RT^{n+1}}-\epsilon^{n}\frac{P^{n}}{RT^{n}}\right)\Big|_{x_{k_{n+1}}}$$
$$+\frac{\tau_1}{\tau}L_h^P(P_j^{n+1},x_l)+\frac{\tau_2}{\tau}L_h^P(P_j^{n},x_l)=\frac{x_{x_l-k_{n+1}}}{h}\Gamma_{c,k_{n+1}-1}^n-\frac{x_l-x_{k_{n+1}-1}}{h}\Gamma_{c,k_{n+1}}^n \tag{4.6}$$

and

$$\frac{x_{k_{n+1}+2}-x_r}{h\tau}\left(\epsilon^{n+1}\frac{P^{n+1}}{RT^{n+1}}-\epsilon^{n}\frac{P^{n}}{RT^{n}}\right)\Big|_{x_{k_{n+1}+1}}$$
$$+\frac{x_r-x_{k_{n+1}+1}}{h\tau}\left(\epsilon^{n+1}\frac{P^{n+1}}{RT^{n+1}}-\epsilon^{n}\frac{P^{n}}{RT^{n}}\right)\Big|_{x_{k_{n+1}+2}}+\frac{\tau_1}{\tau}L_h^P(P_j^{n+1},x_r)+\frac{\tau_2}{\tau}L_h^P(P_j^{n},x_r)$$
$$=-\frac{x_{k_{n+1}+2}-x_r}{h}\Gamma_{c,x_{k_{n+1}+1}}^n-\frac{x_r-x_{k_{n+1}+1}}{h\tau}\Gamma_{c,x_{k_{n+1}+2}}^n. \tag{4.7}$$

The corresponding boundary conditions are defined by

$$\frac{\epsilon_0^{n+1}}{RT_0^{n+1}}P_0^{n+1}-\frac{\epsilon_0^{n}}{RT_0^{n}}P_0^{n}=\frac{2\tau}{h}V_{G,1/2}^nC_{1/2}^n\delta_xP_{1/2}^{n+1}-\tau\Gamma_{c,0}^n-\frac{2\tau}{h}\left[\beta_{11}^0(C_{v,0}^n-C_v^i)+\beta_{12}^0(C_{a,0}^n-C_a^i)\right]$$
$$\frac{\epsilon_{M+1}^{n+1}}{RT_{M+1}^{n+1}}P_{M+1}^{n+1}-\frac{\epsilon_{M+1}^{n}}{RT_{M+1}^{n}}P_{M+1}^{n}=\frac{2\tau}{h}V_{G,M+1/2}^nC_{M+1/2}^n\delta_xP_{M+1/2}^{n+1}-\tau\Gamma_{c,M+1}^n$$
$$-\frac{2\tau}{h}\left[\beta_{11}^L(C_v^o-C_{v,M+1}^{n+1})+\beta_{12}^L(C_a^o-C_{a,M+1}^n)\right]. \tag{4.8}$$

An almost tridiagonal finite volume system of the pressure equation is defined by (4.2)–(4.8).

For the vapor equation, we have the interface condition

$$\left[V_G P_x C_v + D_G C \left(\frac{C_v}{C}\right)_x\right] = 0. \tag{4.9}$$

Let

$$L_h^C(C_{v,j}^{n+1}, x_j) := \frac{1}{h}\left(D_{G,j+1/2}^{n+1} C_{j+1/2}^{n+1} \delta_x \left(\frac{C_{v,j+1/2}^{n+1}}{C_{j+1/2}^{n+1}}\right) - D_{G,j-1/2}^{n+1} C_{j-1/2}^{n+1} \delta_x \left(\frac{C_{v,j}^{n+1}}{C_j^{n+1}}\right)\right]$$
$$+ \frac{1}{h}\left(V_{G,j+1/2}^{n+1} V_{j+1/2}^{n+1} C_{v,j+1/2}^{n+1} - V_{G,j-1/2}^{n+1} V_{j-1/2}^{n+1} C_{v,j-1/2}^{n+1}\right), \quad j = 1, 2, \ldots, k_{n+1} - 1, k_{n+1} + 2, \ldots, M. \tag{4.10}$$

The discrete vapor equations are defined by

$$\frac{\epsilon_j^{n+1} C_{v,j}^{n+1} - \epsilon_j^n C_{v,j}^n}{\tau} = L_h^C(C_{v,j}^{n+1}, x_j) - \Gamma_{c,j}^n, \quad j = 1, 2, \ldots, k_n, k_{n+1} + 2, \ldots, M, \tag{4.11}$$

at regular mesh points and

$$\frac{\epsilon_j^{n+1} C_{v,j}^{n+1} - \epsilon_j^n C_{v,j}^n}{\tau} + \frac{\tau_1}{\tau} L_h^C(C_{v,j}^{n+1}, x_j) + \frac{\tau_2}{\tau} L_h(C_{v,j}^n, x_j) = -\Gamma_{c,j}^n, \quad j = k_n + 1, \ldots, k_{n+1} - 1, \tag{4.12}$$

around the interface. By taking the same approach as used for the pressure equation, we obtain two more discrete equations at (x_l, t_{n+1}) and (x_r, t_{n+1}) defined by

$$\frac{x_{k_{n+1}} - x_l}{h\tau}\left(\epsilon^{n+1} C_v^{n+1} - \epsilon^n C_v^n\right)\Big|_{x_{k_{n+1}-1}} + \frac{x_l - x_{k_{n+1}-1}}{h\tau}\left(\epsilon^{n+1} C_v^{n+1} - \epsilon^n C_v^n\right)\Big|_{x_{k_{n+1}}} + \frac{\tau_1}{\tau} L_h^C(C_{v,j}^{n+1}, x_l) + \frac{\tau_2}{\tau} L_h^C(C_{v,j}^n, x_l)$$
$$= -\frac{x_{k_{n+1}} - x_l}{h} \Gamma_{c,k_{n+1}-1}^n - \frac{x_l - x_{k_{n+1}-1}}{h} \Gamma_{c,k_{n+1}}^n \tag{4.13}$$

and

$$\frac{x_{k_{n+1}+2} - x_r}{h\tau}\left(\epsilon^{n+1} C_v^{n+1} - \epsilon^n C_v^n\right)\Big|_{x_{k_{n+1}+1}} + \frac{x_r - x_{k_{n+1}+1}}{h\tau}\left(\epsilon^{n+1} C_v^{n+1} - \epsilon^n C_v^n\right)\Big|_{x_{k_{n+1}+2}}$$
$$+ \frac{\tau_1}{\tau} L_h^C(C_{v,j}^{n+1}, x_r) + \frac{\tau_2}{\tau} L_h^C(C_{v,j}^n, x_r)$$
$$= -\frac{x_{k_{n+1}+2} - x_r}{h} \Gamma_{c,x_{k_{n+1}+1}}^n - \frac{x_r - x_{k_{n+1}+1}}{h\tau} \Gamma_{c,x_{k_{n+1}+2}}^n. \tag{4.14}$$

The corresponding boundary conditions are given by

$$\epsilon_0^{n+1} C_{v,0}^{n+1} - \epsilon_0^n C_{v,0}^n = \frac{2\tau}{h}\left[V_{G,1/2}^{n+1} \delta_x P_{1/2}^{n+1}(C_{v,1}^{n+1} + C_{v,0}^{n+1}) + D_{G,1/2}^{n+1} C_{1/2}^{n+1} \delta_x \left(\frac{C_{v,1/2}^{n+1}}{C_{1/2}^{n+1}}\right)\right]$$
$$- \frac{2\tau \beta_{21}^0}{h}(C_{v,0}^{n+1} - C_v^i) - \tau \Gamma_{c,0}^n, \tag{4.15}$$

at $x = 0$, and

$$\epsilon_{M+1}^{n+1} C_{v,M+1}^{n+1} - \epsilon_{M+1}^n C_{v,M+1}^n = \frac{2\tau}{h} V_{G,M+1/2}^{n+1} \delta_{P,M+1/2}^{n+1}(C_{v,M+1}^{n+1} + C_{v,M+1}^{n+1})$$
$$+ \frac{2\tau}{h} D_{G,M+1/2}^{n+1} C_{M+1/2}^{n+1} \delta_x \left(\frac{C_{v,M+1}^{n+1}}{C_{M+1}^{n+1}}\right) - \frac{2\tau \beta_{21}^L}{h}(C_v^o - C_{v,M+1}^{n+1}) - \tau \Gamma_{c,M+1}^n \tag{4.16}$$

at $x = L$. An almost tridiagonal finite volume system for the vapor equation is obtained from (4.11)–(4.16).

We present the splitting algorithm below.

Algorithm II. At each time step,

- Step 1. The free water content W_j^{n+1} is first obtained by solving the discrete water equation (4.1). Then the parameters are updated by $\epsilon_j^{n+1} = \epsilon(W_j^{n+1})$, $\kappa_s^{n+1} = \kappa_s(W_j^{n+1})$ and $C_s^{n+1} = C_s(W^{n+1})$ using (2.5), (2.9) and (2.11), respectively. Consequently, D_G^{n+1} and V_G^{n+1} are updated.
- Step 2. Apply Algorithm I for solving the discrete temperature system in (3.1), (3.17) and (3.18) with a moving interface to get the finite volume solution T_j^{n+1} and the interface location α_{n+1}.

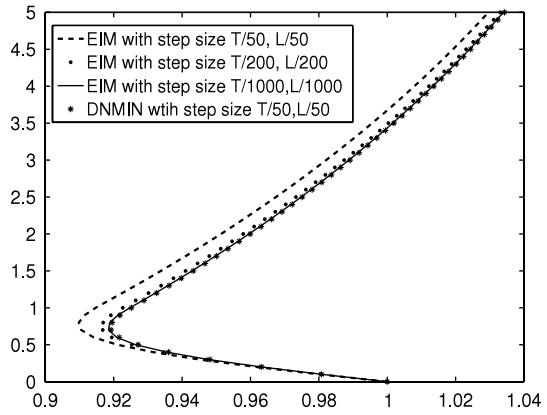

Fig. 2. The comparison of interface locations.

- Step 3. The discrete pressure system (4.2)–(4.8). is solved for the pressure P_j^{n+1} and the mixture gas concentration is updated by $C_j^{n+1} = P_j^{n+1}/(RT_j^{n+1})$.
- Step 4. Finally, the discrete vapor system (4.11)–(4.16) is solved to obtain $C_{v,j}^{n+1}$. The air concentration is updated by $C_{a,j}^{n+1} = C_j^{n+1} - C_{v,j}^{n+1}$.

5. Numerical results

In this section, we present two numerical examples. One is an artificial Stefan problem and other one is a practical clothing assembly model with 10 pile polyester batting and two different covers, laminated and nylon. All computations are performed with Matlab.

5.1. A simple example

Consider a classical two-phase Stefan problem in one dimensional space [27], defined by

$$\frac{\partial u_1}{\partial t} = \sigma_1 \frac{\partial^2 u_1}{\partial x^2}, \quad 0 < x < \alpha(t),\ 0 < t \le T, \tag{5.1}$$

$$\frac{\partial u_2}{\partial t} = \sigma_2 \frac{\partial^2 u_2}{\partial x^2}, \quad \alpha(t) < x < L,\ 0 < t \le T, \tag{5.2}$$

with the initial and boundary condition

$$\begin{aligned}
&u_1(0,t) = g_1(t), \qquad u_1(\alpha(t),t) = 0, \quad 0 < t \le T,\\
&u_2(L,t) = g_2(t), \qquad u_2(\alpha(t),t) = 0, \quad 0 < t \le T,\\
&\alpha(0) = b, \quad 0 \le b \le L,\\
&u_1(x,0) = f_1(x), \quad 0 \le x \le b, \qquad u_2(x,0) = f_2(x), \quad b \le x \le L\\
&\frac{\partial \alpha}{\partial t} = -\kappa_1 \frac{\partial u_1}{\partial x}(\alpha(t),t) + \kappa_2 \frac{\partial u_2}{\partial x}(\alpha(t),t), \quad 0 < t \le T.
\end{aligned} \tag{5.3}$$

Here we take

$$\begin{aligned}
&L = 2, \qquad T = 5, \qquad b = 1\\
&\sigma_1 = 5, \qquad \sigma_2 = 10, \qquad \kappa_1 = \frac{1}{10}, \qquad \kappa_2 = \frac{3}{10},\\
&g_1(t) = 1, \qquad f_1(x) = f_2(x) = 1 - x;\\
&g_2(t) = \begin{cases} -0.25, & 0 < t \le 1\\ -\dfrac{3}{8}\left(\cos \pi t + \dfrac{5}{3}\right), & 1 < t \le 5. \end{cases}
\end{aligned}$$

Table 1
Numerical errors for u and $\alpha(t)$.

M	$E_M(u)$	Ratio	$E_M(\alpha)$	Ratio
30	6.1010e−003	null	4.9011e−003	null
60	1.5021e−003	3.9620	1.4000e−003	3.4353
120	2.8280e−004	5.4749	2.7296e−004	5.1740
240	7.0080e−005	4.0353	6.7672e−005	4.0337
480	1.7502e−005	4.0042	1.6914e−005	4.0010

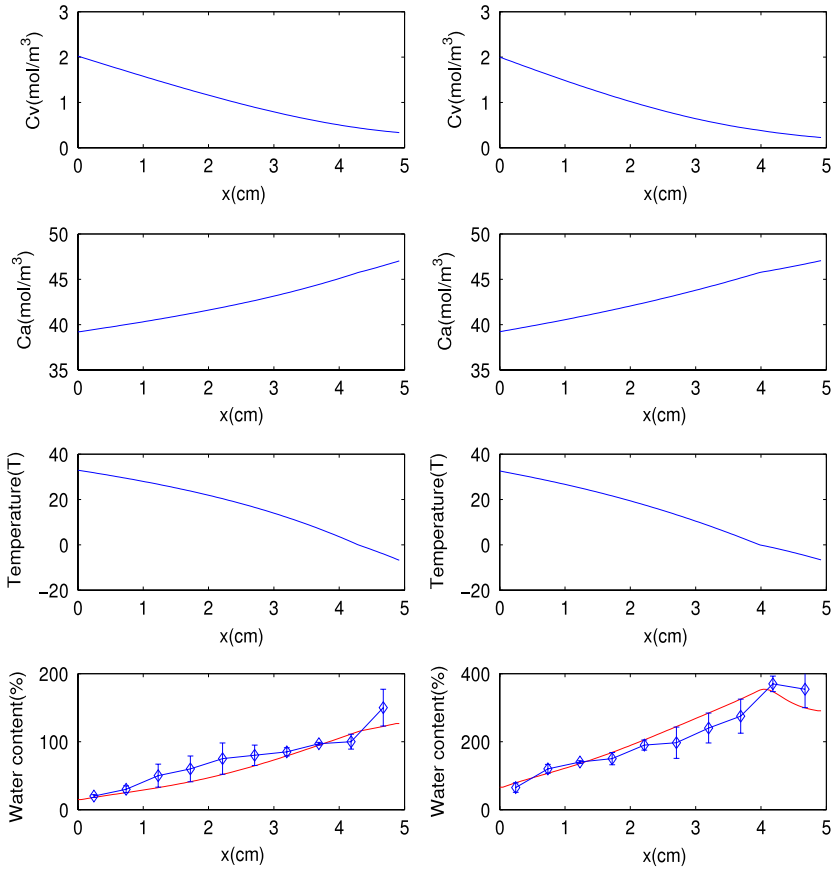

Fig. 3. Numerical results for 10 piles polyester batting sandwiched by two layers of nylon fabric.

We apply Algorithm I (DNMIM) proposed in Section 3 for solving the above Stefan problem. For comparison, an explicit/implicit interface method (EIM) is also tested, in which the explicit Euler scheme

$$\frac{\alpha_{n+1}-\alpha_n}{\tau} = -\kappa_1 \frac{\partial u_1}{\partial x}(\alpha_n, t_n) + \kappa_2 \frac{\partial u_2}{\partial x}(\alpha_n, t_n) \tag{5.4}$$

is used for the interface equation and the implicit Euler scheme is used for the discretization of the Stefan equation.

We present in Fig. 2 the moving interface locations with different mesh size h and time step τ. Clearly the interface location obtained by the proposed algorithm with $h = L/50$ and $\tau = T/50$ is as good as the result obtained by the explicit/implicit method with $h = L/1000$ and $\tau = T/1000$, while the interface location obtained by the explicit/implicit method with $h = L/50$ and $\tau = T/50$ is less accurate. The inaccuracy of the scheme EIM in (5.4) is mainly due to its explicit, which fails to well predicate the speed of propagation. We define two error functions by

$$E_M(u) = \max_{1\le n\le N} \max_j |u(x_j, t_n) - u_j^n|,$$
$$E_M(\alpha) = \max_{1\le n\le N} |\alpha(t_n) - \alpha_n|$$

where $(u(x,t), \alpha(t))$ is a solution obtained by the proposed method with a finer mesh, $\tau = T/10000$ and $h = L/3840$, and (u_j^n, α_n) is the corresponding numerical solution by the proposed numerical method with $\tau = T/5000$ and different mesh

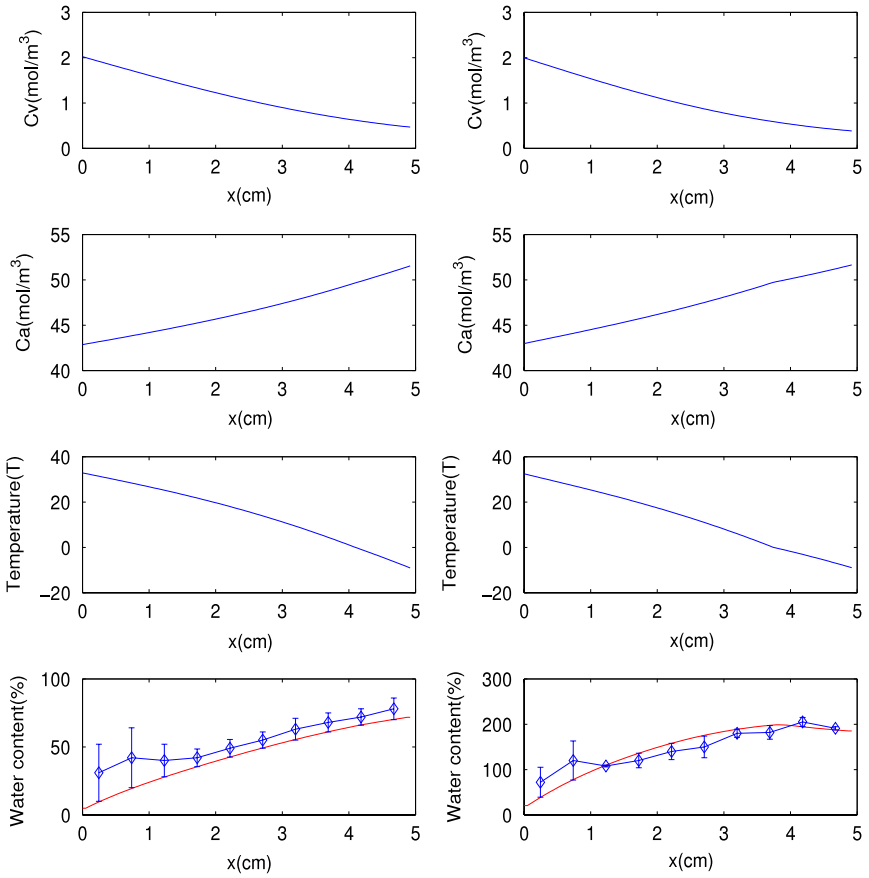

Fig. 4. Numerical results for 10 piles polyester batting sandwiched by two layers of laminated fabric.

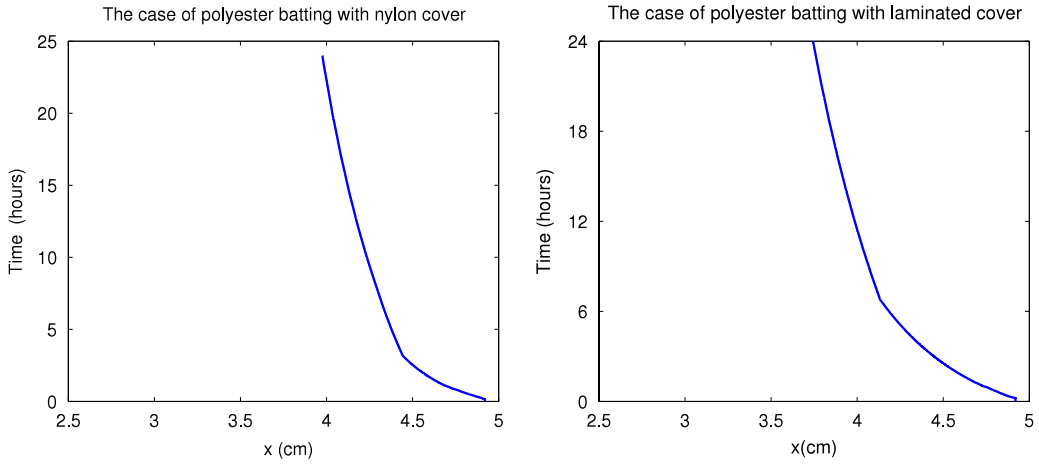

Fig. 5. The location of moving interface in 24 h.

size h. We present in Table 1 numerical errors for both the solution u and the interface location α. We can see clearly from Table 1 the second-order convergence of the method for both u and α in spatial direction.

5.2. Clothing assemblies

The second example is to study the air–vapor–heat transfer in a clothing assembly with a porous batting sandwiched by two covering layers. Two cases to be considered are:

- Case I: 10 pile polyester batting with laminated cover;
- Case II: 10 pile polyester batting with nylon cover;

The values of physical parameters can be found in [7,8]. Experimental measurements for water accumulated in the cloth assembly were given in [24]. Here all numerical results are obtained by the splitting finite volume method with $\tau = 20s$, $h = L/100$. To confirm our numerical results, the splitting finite volume method with smaller time and spatial steps was also tested. Our numerical experiments show that the scheme is stable when the time step is smaller than 20 s.

We present in Fig. 3 numerical results of the vapor concentration C_v, air concentration C_a, temperature T, water content W for Case I at 8 h and 24 h. The comparison between numerical results of water content and experimental measurements [24] are also given in the last subfigures. The corresponding numerical results for Case II are presented in Fig. 4. The moving interface locations for both Case I and case II are given in Fig. 5. Some observations are made below.

Due to the discontinuity of the conductivity κ, more precisely $\kappa_w = 0.57$ for water ($T \geq T_f$) and $\kappa_w = 2.13$ for ice ($T \leq T_f$), the temperature is not smooth (T_x is discontinuous). Since the amount of water content (W) at 24 h is much larger than the amount at 8 h, the discontinuity of T_x at 24 h is clearer in both cases. Physically, the gradient of the pressure P_x is continuous. Therefore, by noting the fact $P = RCT$, the mixture gas concentration C is not smooth at the interface. So we can see from the second subfigures of Figs. 3 and 4 for 24 h the slightly non-smoothness of the air concentration (C_a) at the interface since $C_v \ll C_a$ and $C = C_a + C_v \sim C_a$.

Numerical simulations for both cases were done by a splitting finite difference method [8] and finite volume method [10] without any approximation to the interface. It has been noted that such schemes are not only less accurate around the interface, and also are more restrictive at time step. Numerical simulations in [8,10] show that schemes are stable only when the time steps are less than 5 s and 10 s, respectively, while the proposed methods shows almost unconditionally stable.

We also see from Fig. 5 that the interface is moving monotonically from right to left in bath cases and compared with the nylon cover, the interface for the case with the laminated cover goes a little more far away. This is mainly because the nylon cover provides a higher resistance to vapor moving out, which leads to more water accumulated and higher temperature in the batting area, particularly near the outer cover.

References

[1] M.K. Choudhary, K.C. Karki, S.V. Patankar, Mathematical modeling of heat transfer, condensation, and cappilary flow in porous insulation on a cold pipe, Int. J. Heat Mass Transfer 47 (2004) 5629–5638.
[2] J. Fan, Z. Luo, Y. Li, Heat and moisture transfer with sorption and condensation in porous clothing assemblies and numerical simulation, Int. J. Heat Mass Transfer 43 (2000) 2989–3000.
[3] W.R. Foss, C.A. Bronkhorst, K.A. Bennett, Simultaneous heat and mositure transport in paper sheets during moisture sorption from humid air, Int. J. Heat Mass Transfer 46 (2002) 2875–2886.
[4] G. Henrique, D. Santos, N. Mendes, Combined heat, air and moisture (HAM) transfer model for porous building materials, J. Build. Phys. 32 (2009) 203–220.
[5] C.V. Le, N.G. Ly, R. Postle, Heat and Moisture Transfer in Textile Assemblies, Text. Res. J. 65 (1995) 203–212.
[6] A. Cheng, H. Wang, An error estimate on a Galerkin method for modeling heat and moisture transfer in fibrous insulation, Numer. Methods Partial Differential Equations 24 (2008) 504–517.
[7] J. Fan, X. Cheng, X. Wen, W. Sun, An improved model of heat and moisture transfer with phase change and mobile condensates in fibrous insulation and comparison with experimental results, Int. J. Heat Mass Transfer 47 (2004) 2343–2352.
[8] H. Huang, C. Ye, W. Sun, Moisture transport in fibrous clothing assemblies, J. Eng. Math. 61 (2008) 35–54.
[9] B. Li, W. Sun, Y. Wang, Global existence of weak solution to the heat and moisture transport system in fibrous porous media, J. Differ. Equ. 249 (2010) 2618–2642.
[10] C. Ye, H. Huang, J. Fan, W. Sun, Numerical study of heat and moisture transfer in textile materials by a finite volume method, Commun. Comput. Phys. 4 (2008) 929–948.
[11] C. Ye, B. Li, W. Sun, Quasi-steady state and steady state models for heat and moisture transport in textile assemblies, Proc. R. Soc. Lond. Ser. A Math. Phys. Eng. Sci. 466 (2010) 2875–2896.
[12] X. He, T. Lin, Y. Lin, Immersed finite element methods for elliptic interface problems with non-homogeneous jump conditions, Int. J. Numer. Anal. & Modeling 8 (2011) 284–301.
[13] R.J. LeVeque, Z. Li, The immersed interface method for elliptic equations with discontinuous coefficients and singular sources, SIAM J. Numer. Anal. 31 (1994) 1019–1044.
[14] Z. Li, K. Ito, The Immersed Interface Method: Numerical Solutions of PDEs Involving Interfaces and Irregular Domains, SIAM, 2006.
[15] J. Sethian, A Level Set Methods and Fast Marching Methods, 2nd ed., Cambridge University Press, 1999.
[16] S. Zhu, G. Yuan, W. Sun, Convergence and stability of explicit/implicit schemes for parabolic equations with discontinuous coefficients, Int. J. Numer. Anal. & Modeling 1 (2004) 131–146.
[17] W. Huang, W. Sun, Variational mesh adaptation II: error estimates and monitor functions, J. Comput. Phys. 184 (2003) 619–648.
[18] H. Tang, T. Tang, Adaptive mesh methods for one- and two-dimensional hyperbolic conservation laws, SIAM J. Numer. Anal. 41 (2003) 487–515.
[19] Z. Li, Immersed interface method for moving interface problems, Numer. Algorithms. 14 (1994) 269–293.
[20] Z. Li, T. Lin, Y. Lin, R.C. Rogers, An immersed finite element space and its approximation capability, Numer. Methods Partial Differential Equations 20 (2004) 338–367.
[21] G. Bao, W. Sun, A Fast algorithm for electromagnetic scattering from a large cavity, SIAM J. Sci. Comput. 27 (2005) 553–574.
[22] G.H. Meyer, On a free interface problem for linear ordinary differential equations and the one-phase Stefan problem, Numer. Math. 16 (1970) 248–267.
[23] H. Han, X. Wu, A fast numerical method for the Black–Scholes equation of American options, SIAM J. Numer. Anal. 41 (2003) 2081–2095.
[24] J. Fan, X. Cheng, Y.S. Chen, An experimental investigation of moisture absoption and condensation in fibrous insulations under low temperature, Exp. Therm. Fluid Sci. 27 (2002) 723–729.
[25] F.E. Jones, Evaporation of Water, Lewis Publishers Inc., Michigan, 1992, pp. 25-43.
[26] S.G. Gupta, The Classical Stefan Problem Basic Concepts, Modelling and Analysis, vol. 45, Elsevier, 2003.
[27] M. Mori, A finite element method for solving the two phase Stefan problem in one space dimension, RIMS 13 (2008) 723–753.